



## The Cu–Sn phase diagram part II: New thermodynamic assessment

D. Li<sup>a,\*</sup>, P. Franke<sup>a</sup>, S. Fürtauer<sup>b</sup>, D. Cupid<sup>a</sup>, H. Flandorfer<sup>b</sup>

<sup>a</sup>Karlsruhe Institute of Technology, Institute for Applied Materials – Applied Materials Physics, Karlsruhe, Germany

<sup>b</sup>Institute of Inorganic Chemistry/Materials Chemistry, University of Vienna, Vienna, Austria

### ARTICLE INFO

#### Article history:

Received 11 May 2012

Received in revised form

14 September 2012

Accepted 4 October 2012

Available online 30 November 2012

#### Keywords:

B. Order/disorder transformations

E. Phase diagram

E. Prediction

### ABSTRACT

A thermodynamic description for the Cu–Sn system was developed using the CALPHAD approach taking into account all available literature data as well as the experimental results presented in Part I of this work. The higher order transformation from the disordered A2 phase to the ordered DO<sub>3</sub> phase has been described using the (Cu,Sn)<sub>0.25</sub>(Cu,Sn)<sub>0.25</sub>(Cu,Sn)<sub>0.25</sub>(Cu,Sn)<sub>0.25</sub> four-sublattice model for the first time. The calculated A2/DO<sub>3</sub> phase boundary is in good agreement with literature data. Additionally, the enthalpy of mixing of the liquid phase and the activity of Cu and Sn in the liquid alloys are well reproduced and enthalpies of formation of solid alloys and the activity of Sn in the (Cu) solid solution are calculated.

© 2012 Elsevier Ltd. All rights reserved.

### 1. Introduction

The Cu–Sn alloys, also called tin bronzes, have been widely used since the Bronze Age due to their high strength, high wear resistance, good corrosion resistance and easy casting properties. A renewed interest for investigating the Cu–Sn system has been expressed due to the development of the microelectronic industry as well as the drive to produce lead-free solders [1–3]. More recently, Cu–Sn alloys have been found to be one of the potential anode materials for replacing the traditional carbon based anode in the lithium ion battery because of their relatively high theoretical charge densities. Additionally, Cu can form a matrix which can accommodate the extensive volume changes occurring during the charge–discharge cycles from de-intercalation and intercalation of Li [4–8]. Although the Cu–Sn phase diagram seems to be well investigated and widely accepted, there are still doubts concerning the phase relations of the high temperature bcc based  $\beta$  and  $\gamma$  phases. They have been addressed and clarified by doing new experiments in Part I of this paper. However, the existing thermodynamic descriptions of these phases [9–11] are no longer consistent with the latest experimental results shown in Part I. Therefore, the aim of this work is to generate a new

thermodynamic description of the Cu–Sn system taking into account our experimental work detailed in Part I.

### 2. Thermodynamic assessments of the Cu–Sn system

The phase diagram of the Cu–Sn system was constructed in 1944 by Raynor [12]. Since then, only minor modifications and refinements to the phase relations have been proposed and critical evaluations of the literature performed by Hansen [13], Hansen and Anderko [14] and Saunders [15,16].

Thermodynamic descriptions of the Cu–Sn system have been optimized and developed by Shim et al. [9], Miettinen [10], Liu et al. [17], Gierlotka et al. [11], and Li et al. [18]. Other thermodynamic descriptions exist which have made small modifications of previous descriptions. For example, the description of Lee [19] is based on Ref. [18], and that of Wang et al. [20] is based on the description of Moon et al. [21], who, in turn, uses the thermodynamic description of Ref. [9]. The main difference between the various thermodynamic assessments is the thermodynamic model used to describe the  $\beta$  (A2) and  $\gamma$  (DO<sub>3</sub>) phases between 12 and 30 at.% Sn and in the temperature range from 800 to 1100 K. Miettinen [10] used the substitutional solution model to describe the  $\gamma$  phase, which was adopted in the assessment of Li et al. [18]. Shim et al. [9] described the  $\gamma$  phase using a two-sublattice model as (Cu,Sn)<sub>0.75</sub>(Cu,Sn)<sub>0.25</sub> which was adopted by Gierlotka et al. [11]. Lee [19] also used the thermodynamic parameters of Shim [9] but omitted the  $\gamma$  phase, choosing instead to model only the  $\beta$  phase in the composition range of these two phases. Liu et al. [17], based on the results of differential scanning calorimetry (DSC), high-temperature electron

\* Corresponding author. Karlsruhe Institute of Technology (KIT), Institute for Applied Materials – Applied Materials Physics (IAM-AWP), Hermann-von-Helmholtz-Platz 1, Building 681, 76344 Eggenstein-Leopoldshafen, Germany. Tel.: +49 721 608 22872; fax: +49 721 608 24567.

E-mail address: [dajian.li@kit.edu](mailto:dajian.li@kit.edu) (D. Li).

diffraction (HTED), and high temperature X-ray diffraction (HTXRD) measurements, modeled a disordered A2 to B2 ordered phase transformation.

Since Part I of this paper has shown that a higher order transformation exists between the disordered  $\beta$  phase and the ordered  $\gamma$  phase, the aim of this work is to produce a thermodynamic description of the Cu–Sn system which calculates this higher order phase transformation.

### 3. Literature data

As the phase diagram data as well as information on compounds in the Cu–Sn system have already been discussed in Part I of this work, only the thermodynamic and thermochemical data for the Cu–Sn system will be presented in the following review.

Critical evaluations of the experimental data on the Cu–Sn system have been performed by Hansen and Anderko [14], Hultgren and Desai [22], Hultgren [23], and Saunders and Miodownik [16]. However, due to the large amount of investigations performed in the Cu–Sn system, some of the critical reviews omit some literature data. An extensive review of the Cu–Sn system has also been presented in the thermodynamic assessment of Shim et al. [9]. Since 1996, only Flandorfer et al. [24,25] have performed experimental work on the Cu–Sn system by measuring the enthalpies of formation of the compounds and enthalpies of mixing of the liquid phase.

The integral mixing enthalpies of liquid Cu–Sn alloys have been measured several times in the temperature range from 723 to 1523 K covering the whole composition range [23,25–31]. The integral mixing enthalpies of the liquid Cu–Sn alloys show slightly positive values at the Sn rich side and a minimum can be found at approximately  $x_{\text{Cu}} = 0.75$ , which corresponds to the stable  $\text{Cu}_3\text{Sn}$  intermetallic phase. Most measurements agree with each other within 1000 J/mol and no temperature dependence could be concluded based on these results. Only the works of Iguchi et al. [31] and Itagaki and Yazawa [29], respectively, show more exothermic and less exothermic behavior when compared to the other works. It should be noted that the measurements of Iguchi et al. [31] were performed at high temperature (1493 K), which usually means that less exothermic mixing behavior is expected. Flandorfer et al. [25] systematically investigated the integral mixing enthalpies of the Cu–Sn liquid alloys in the temperature range from 773 to 1523 K and found drastic changes in the mixing enthalpy values between 773 and 993 K but less temperature dependence at higher temperatures.

The activities of Cu or Sn in the liquid phase were measured by Refs. [32–35] using vapor pressure measurements and by Refs. [36,37] using the electromotive force (e.m.f.) method. The literature data cover the temperature range from 1073 to 1593 K as well as the whole composition range, and are in good agreement with each other.

The enthalpies of formation for the Cu–Sn solid alloys have been reported by different authors [24,38–41] using calorimetric measurements. Assessed values by Hultgren [23] could also be considered for the optimization.

The activity of Sn in the (Cu) solid solution was measured by Predel and Schallner [42] and Sommer et al. [43] using the e.m.f. method. Alcock and Jacob [44] also determined the activity of Sn in the (Cu) solid solution by vapor pressure measurements. The results from Alcock and Jacob [44] and Sommer et al. [43] are in agreement with each other while those of Predel and Schallner [42] are much lower.

The limiting partial enthalpies of formation of Cu in liquid Sn has been summarized by Yassin and Castanet [45] up to 2000 K and show a slightly positive temperature dependence. Flandorfer et al.

[24] measured the limiting partial enthalpies using solution calorimetry and found a stronger positive temperature dependence than Yassin and Castanet [45].

Table 1 summarizes the experimental work from the literature which was assessed for the present thermodynamic optimization of the Cu–Sn system.

### 4. Thermodynamic modeling

The thermodynamic descriptions of the pure elements were taken from the SGTE 5.1 database supplied with the Thermo-Calc<sup>®</sup> version 5 software. The  $\epsilon$ - $\text{Cu}_3\text{Sn}$ ,  $\delta$ - $\text{Cu}_{41}\text{Sn}_{11}$  and  $\zeta$ - $\text{Cu}_{10}\text{Sn}_3$  phases were modeled as stoichiometric phases. The Gibbs energy of the stoichiometric phase  $\text{Cu}_p\text{Sn}_q$  with  $p$  and  $q$  as stoichiometric coefficients is expressed as:

$$G_m^{\text{Cu}_p\text{Sn}_q}(T) - p^0H_{\text{Cu}}^\varphi - q^0H_{\text{Sn}}^\varphi = \Delta_f G_{\text{Cu}_p\text{Sn}_q}(T) + p \cdot \text{GHSERCU}(T) + q \cdot \text{GHSERSN}(T) \quad (1)$$

where  $^0H_{\text{Cu}}^\varphi$  and  $^0H_{\text{Sn}}^\varphi$  are the enthalpies of pure Cu and Sn in their stable states  $\varphi$  at 298.15 K respectively,  $\Delta_f G_{\text{Cu}_p\text{Sn}_q}$  is the standard Gibbs free energy of formation of the stoichiometric compound from the pure elements, and GHSERCU and GHSERSN are the Gibbs free energies of the pure elements Cu and Sn referred to the enthalpy of their stable states  $\varphi$  at 298.15 K.

The liquid,  $\alpha$ -(Cu) and disordered A2 phases were described using the substitutional solution model where the Gibbs free energy is given as:

$$G_m = \text{srf}G_m + \text{cfg}G_m + {}^E G_m \quad (2)$$

where  $\text{srf}G$  represents the surface of reference,  $\text{cfg}G$  represents the contribution to the total Gibbs free energy resulting from the configurational entropy of mixing, and  ${}^E G_m$  describes the excess Gibbs energy of mixing. For substitutional solutions in the binary Cu–Sn system, the surface of reference is modeled as:

$$\text{srf}G = x_{\text{Cu}} {}^0G_{\text{Cu}}^\varphi + x_{\text{Sn}} {}^0G_{\text{Sn}}^\varphi \quad (3)$$

and the contribution of the configurational entropy of mixing to the Gibbs free energy is expressed as:

$$\text{cfg}G_m = RT(x_{\text{Cu}} \ln x_{\text{Cu}} + x_{\text{Sn}} \ln x_{\text{Sn}}) \quad (4)$$

where  $x_{\text{Cu}}$  and  $x_{\text{Sn}}$  are the mole fractions of Cu and Sn respectively. The excess Gibbs free energy of mixing was modeled using the Redlich–Kister polynomials [54] as:

$${}^E G_m = x_{\text{Cu}} x_{\text{Sn}} \sum_p {}^V L_{\text{Cu,Sn}}(x_{\text{Cu}} - x_{\text{Sn}})^p \quad (5)$$

The  $\eta$ - $\text{Cu}_6\text{Sn}_5\text{-H}$  and low temperature  $\eta'$ - $\text{Cu}_6\text{Sn}_5\text{-L}$  phases were modeled using the compound energy formalism expressed in the sublattice model in which the Gibbs energy of a phase is expressed as:

$$G_m = \text{srf}G_m + \text{cfg}G_m + {}^E G_m = \sum \left( \prod y_i^s \Delta_f^0 G_{\text{end}} \right) + RT \sum_s \sum_i a^s y_i^s \ln y_i^s + {}^E G_m \quad (6)$$

where  $\Delta_f^0 G_{\text{end}}$  is the Gibbs energy of formation of the end-members,  $a^s$  is the stoichiometric coefficient of sublattice  $s$ ,  $y_i^s$  is

**Table 1**  
Experimental thermodynamic data in the Cu–Sn system.

Properties	Ref.	Experimental technique	QM	Comments
$\Delta_{\text{mix}}H_m$ at 997 K	[27]	HT calorimetry	Y	
$\Delta_{\text{mix}}H_m$ at 1440 K	[30]	HT calorimetry	Y	
$\Delta_{\text{mix}}H_m$ at 1493 K	[31]	Isothermal calorimetry	N	More exothermic than other data
$\Delta_{\text{mix}}H_m$ at 1373 K	[29]	Single adiabatic wall calorimetry	N	Less exothermic than other data
$\Delta_{\text{mix}}H_m$ at 1063 K	[28]	HT calorimetry	Y	
$\Delta_{\text{mix}}H_m$ at 723 K	[23]	Assessed	Y	
$\Delta_{\text{mix}}H_m$ at 1400 K	[23]	Assessed	Y	
$\Delta_{\text{mix}}H_m$ at 723 K	[26]	Sn solution calorimetry	N	Showed more exothermic values which may be due to temperature dependence. However, insufficient data presented.
$\Delta_{\text{mix}}H_m$ at 773, 973, 1173, 1373, 1523 K	[25]	HT calorimetry	Y	Showed more exothermic values at 773 K which may due to temperature dependence. However, insufficient data presented.
Activity of Cu and Sn in liquid at 1573 K	[33]	Knudsen cell-mass filter combination	Y	
Activity of Cu and Sn in liquid at 1400 K	[23]	Assessed	Y	
Activity of Cu and Sn in liquid at 1593 K	[35]	Knudsen cell mass spectrometry	Y	Knudsen cell equipped with a T.O.F. mass spectrometer
Activity of Cu and Sn at 1300 K	[44]	Knudsen cell mass spectrometry	Y	
Activity of Cu and Sn at 1403 K	[34]	Knudsen cell	Y	
Activity of Sn in liquid at 1073 K	[36]	e.m.f.	Y	
Activity of Sn in liquid at 1173–1373 K	[37]	e.m.f.	Y	The measurements were performed in the temperature interval 1173–1373 K. However, the temperature for each measurement was not specified.
Enthalpy of formation for solid alloys at 298 K	[24]	Solution calorimetry	Y	Cu <sub>3</sub> Sn, Cu <sub>41</sub> Sn <sub>11</sub> , Cu <sub>6</sub> Sn <sub>5</sub> _H phases investigated.
Enthalpies of formation for solid alloys at 723 K	[23]	Assessed	Y	
Enthalpy of formation for solid alloys at 723 K	[40]	Sn solution calorimetry	Y	
Enthalpy of formation for solid alloys at 273 K	[39]	Sn solution calorimetry	Y	
Enthalpy of formation for Cu <sub>3</sub> Sn at 298 K	[38]	Br <sub>2</sub> /KBr Solution calorimetry	Y	
Enthalpy of formation for Cu <sub>6</sub> Sn <sub>5</sub> _L	[41]	Sn solution calorimetry at 623 K.	Y	Determined also HT/LT structure-transformation energy
Infinite dilution partial enthalpy of mixing of Cu	[45]	Summarized all previous data	N	Data showed a slight temperature dependence, which was not taken into account.
Infinite dilution partial enthalpy of mixing of Cu	[24]	Solution calorimetry	N	Data showed a slight temperature dependence which was not taken into account.
Invariant reactions	[16]	Assessed	N	Data used only for comparison.
Phase boundary between L + (Cu)	[46]	Microprobe analysis	Y	
Liquidus, solidus, invariant reactions	[47]	Cooling curve method	Y	
Phase boundary of fcc phase and adjacent liquid or bcc phase	[48]	Micrographic and cooling method	Y	
Liquidus and solidus	[49]	Cooling method	Y	
Phase diagram in the vicinity of the bcc phase	[50]	Cooling method	Y	
Phase diagram	[51]	DTA, temperature–electric resistance measurement, temperature dilatation measurement, microscopic examination, XRD	Y	
Phase diagram	[52]	Cooling method	Y	
Phase boundary of (Cu) at low temperature	[53]	Mechanical alloying, annealing, XRD, LOM	Y	
Activity of Sn in (Cu)	[44]	Gas–solid equilibrium technique	Y	
Activity of Sn in (Cu)	[42]	Solid state e.m.f.	N	Very low value which is not consistent with the phase boundary.
Activity of Sn in (Cu)	[43]	Solid state e.m.f.	Y	

QM: quote mode, indicates whether the data are applied for the optimization.

HT calorimetry: high temperature calorimetry.

XRD: X-ray diffraction.

DTA: differential thermal analysis.

e.m.f.: electromotive force measurement.

LOM: light optical microscopy.

the site fraction of species  $i$  on sublattice  $s$ , and  ${}^E G_m$  is the excess Gibbs free energy. The excess Gibbs free energy is modeled as:

$${}^E G_m = \sum_P \prod_{s \neq r} y_i^s \cdot y_A^r y_B^r L_{A,B,C,\dots} \quad (7)$$

where  $P$  represents the condition where mixing of components  $A$  and  $B$  takes place on sublattice  $r$  whereas all other  $(s-1)$  sublattices are singly occupied.

In the present work, a three sublattice model Cu<sub>0.545</sub>(Cu,Sn)<sub>0.122</sub>Sn<sub>0.333</sub> is used to describe the  $\eta$ -Cu<sub>6</sub>Sn<sub>5</sub>\_H phase. This model was chosen since it could be used to describe the

complete solubility of the  $\eta$  phase from the Cu–Sn binary to the Cu–In binary in the Cu–Sn–In ternary system [55] and was accepted in the COST 531 description [19]. The  $\eta'$  phase is modeled using a two sublattice model as Cu<sub>0.545</sub>(Cu,Sn)<sub>0.455</sub> in order to reproduce the invariant reactions of the  $\eta$  and  $\eta'$  phases with Cu<sub>3</sub>Sn and (Sn) at 462 and 459 K respectively [15].

#### 4.1. The $\beta$ -A2 $\rightarrow$ $\gamma$ -DO<sub>3</sub> higher order phase transformation

The bcc-phase can transform into several ordered structures depending on temperature, composition and the interactions

between the constituents of the phase. These are the B2 and  $\text{DO}_3$  structures which occur for example in the binary systems Fe–Al and Fe–Si. Additional ordered structures are the B32 structure which appears in the Al–Li system and a certain structure which belongs to the space group  $\text{F}\bar{4}3\text{m}$ . In the Cu–Sn system, only the disordered bcc phase and the ordered  $\text{DO}_3$  structure are stable. However, in metastable states, additional ordered structures may occur which can be stabilized by the addition of a third alloying element. Therefore, a more general treatment is desirable which can be extended into higher-order systems in the future.

In order to describe the ordering transition in this system, a four-sublattice model (4SL-model)  $(\text{Cu}, \text{Sn})_{0.25}^{(\text{I})}(\text{Cu}, \text{Sn})_{0.25}^{(\text{II})}(\text{Cu}, \text{Sn})_{0.25}^{(\text{III})}(\text{Cu}, \text{Sn})_{0.25}^{(\text{IV})}$  is used. The roman numerals indicate the sublattice number and each sublattice has a stoichiometric coefficient of 0.25. In the disordered state (A2) of the binary system under consideration, all four sublattices have the same occupation numbers for Cu and Sn, respectively, which are given by the mole fractions of these elements in the solid solution. The B2 and B32 structures are represented in the 4SL-model by two pairs of equivalent sublattices. However, these structures differ in the occupation of their nearest and next-nearest neighbor sites. In the  $\text{DO}_3$  structure, two sublattices are equivalent while each of the other two sublattices has its own occupation number for Cu and Sn,

respectively. Finally, in the  $\text{F}\bar{4}3\text{m}$  state, all four sublattices have different occupation numbers. For this structure, no Strukturbericht symbol is available. Therefore, it is named according to the prototype which is LiMgPdSn [56].

All these ordered structures can be established by considering a 4SL-model consisting of 4 interpenetrating fcc lattices which are displaced by the vectors  $(0, 0, 0)$ ,  $(\frac{1}{2}, \frac{1}{2}, \frac{1}{2})$ ,  $(\frac{1}{4}, \frac{1}{4}, \frac{1}{4})$  and  $(\frac{3}{4}, \frac{3}{4}, \frac{3}{4})$  for sublattice I, II, III, and IV, respectively as shown in Fig. 1. The body centered cube depicted in Fig. 1a has only one half of the lattice parameter of the interpenetrating fcc lattices. These four sublattices correspond also to the Wyckoff positions a, b, c, and d of the space group  $\text{F}\bar{4}3\text{m}$ . Thus, a site in sublattice I is surrounded by 8 nearest neighbors in sublattices III and IV, and has 6 next nearest neighbors in sublattices I and II. In the B2 (Fig. 1b) structure, sublattices I and II are equivalent as well as sublattices III and IV. Two combinations result in the B32 structure: either the equivalent sublattices are I + III and II + IV (Fig. 1c) or alternatively the combination I + IV and II + III. In a binary system A–B the ground states of the B2 and B32 structures have the same stoichiometry (A:B = 1:1) but generally differ in their energy due to different coordination between the nearest and next nearest neighbors for a given lattice site. In the  $\text{DO}_3$  structure the equivalent sublattices are either I + II or III + IV (Fig. 1d), while the other two sublattices

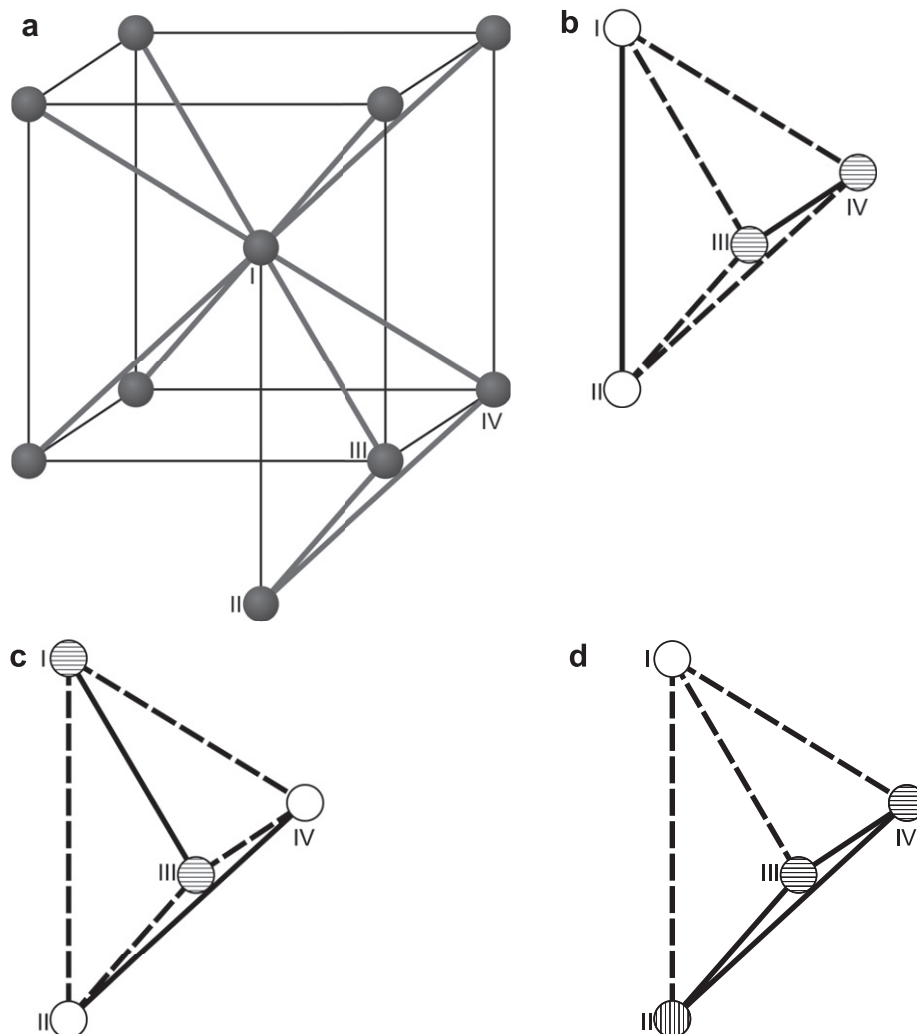


**Fig. 1.** bcc-Based ordered structures: (a) disordered A2 unit cell with one extra atom at the bottom, the lattice parameter of the ordered structures is two times bigger than the A2 unit cell; (b) B2; (c) B32; (d)  $\text{DO}_3$ .

differ from each other as well as they differ from the pair. Only at zero Kelvin at the composition  $A_3B$  or  $AB_3$  of a binary system  $A-B$  can the three sublattices become equivalent in the ground state of the  $D0_3$  structure.

Order–disorder transitions can be treated by various methods. The present work uses the modified compound energy formalism where the parameters are related to the Gibbs energies of ordering of the respective compounds [57]. According to this formalism the Gibbs energy for a phase with an ordering transition is given by:

$$G_m = G_m^{\text{dis}}(x_i) + G_m^{\text{ord}}(y_i^{(s)}) - G_m^{\text{ord}}(x_i) \quad (8)$$

where  $G_m^{\text{dis}}(x_i)$  is the Gibbs energy of the disordered parent solution phase and the last two terms provide the contribution of phase ordering. The function  $G_m^{\text{ord}}(y_i^{(s)})$  is first calculated using the site fractions  $y_i^{(s)}$  of species  $i$  in the respective sublattice  $s$  and then the function  $G_m^{\text{ord}}(x_i)$  is calculated using the mole fractions  $x_i$  instead of the site fractions in all sublattices. When the solution is in its disordered state, the last two terms in the above equation cancel. The function for the ordering contributions is given by:

$$G_m^{\text{ord}}(y_i^{(s)}) = \sum_i \sum_j \sum_k \sum_l y_i^I y_j^{II} y_k^{III} y_l^{IV} G_{ij:kl}^{4SL} + 0.25RT \sum_i \sum_s y_i^{(s)} \ln y_i^{(s)} \quad (9)$$

Generally, this function can have additional excess terms which have been omitted in the present treatment.

In order to calculate the phase diagram with the desired ordering transitions, the set of ordering parameters,  $G_{ij:kl}^{4SL}$ , has to be determined. Ordering in a binary system on a bcc parent lattice has already been analyzed in the literature using the Bragg–Williams–Gorsky formalism [58,59] in which the central model parameters are the bond exchange energies,  $w_1$  and  $w_2$ , between the nearest and next nearest neighbors, respectively. In a systematical study, Inden [59] varied the ratio of these bond exchange energies and calculated the resulting binary phase diagrams. In order to utilize these results in the present work it is necessary to express the Gibbs energies of ordering in terms of the bond exchange energies. The required equations for the compound energies which correspond

to the ground states have already been reported by Hallstedt et al. [60,61] and they are repeated here for the B2, B32, and  $D0_3$  structures as:

$$\begin{aligned} \text{B2: } G_{\text{Cu:Cu:Sn:Sn}}^{4SL} &= G_{\text{Sn:Sn:Cu:Cu}}^{4SL} = -4w_1 \\ \text{B32: } G_{\text{Cu:Sn:Cu:Sn}}^{4SL} &= G_{\text{Cu:Sn:Sn:Cu}}^{4SL} = G_{\text{Sn:Cu:Cu:Sn}}^{4SL} = G_{\text{Sn:Cu:Sn:Cu}}^{4SL} \\ &= -2w_1 - 3w_2 \\ \text{D0}_3: G_{\text{Cu:Cu:Cu:Sn}}^{4SL} &= G_{\text{Cu:Cu:Sn:Cu}}^{4SL} = G_{\text{Cu:Sn:Cu:Cu}}^{4SL} = G_{\text{Sn:Cu:Cu:Cu}}^{4SL} \\ &= G_{\text{Sn:Sn:Sn:Cu}}^{4SL} = G_{\text{Sn:Sn:Cu:Sn}}^{4SL} = G_{\text{Sn:Cu:Sn:Sn}}^{4SL} \\ &= G_{\text{Cu:Sn:Sn:Sn}}^{4SL} = -2w_1 - 1.5w_2 \end{aligned} \quad (10)$$

The LiMgPdSn structure does not have a corresponding compound in a binary system. The sign convention for the bond exchange energies is chosen to comply with the definitions in Refs. [58,59].

## 5. Optimization procedure

The thermodynamic optimization of the Cu–Sn system was performed using the PARROT [62] module of Thermo-Calc<sup>®</sup> and the initial thermodynamic parameters for all phases were taken from the thermodynamic description of the Cu–Sn system from the COST 531 dataset [19]. First, the thermodynamic parameters of the liquid phase were optimized to fit the experimental thermochemical data including the mixing enthalpy and activity data reported by different authors [23,25,27–37]. Second, the parameters of the  $\beta$  phase were modified to remove the inverse miscibility gap which is calculated using the original COST 531 description [19]. Following this step, the parameters of the fcc phase were optimized together with those of the liquid and  $\beta$  phases. The solid phases were then added successively from the Cu-rich side to Sn-rich side and their parameters were optimized to fit the available thermodynamic data, the phase boundaries with already included phases, and the relevant invariant reactions (if existing). In each step, the parameters of the phases which were already included were also optimized in order to improve the fit to the experimental data.

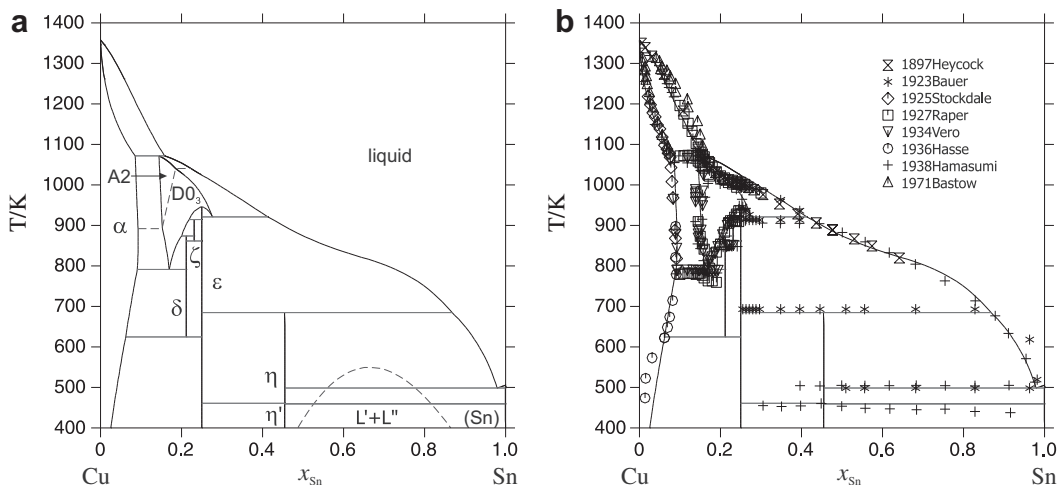


Fig. 2. The Cu–Sn phase diagram: (a) calculated using the present description and (b) with the experimental data from the literature superimposed [46–53].

Since the order/disorder transitions are treated by the modified compound energy formalism [58], the contribution to the Gibbs free energy resulting from ordering is separated from the Gibbs free energy description of the disordered state. In the Cu–Sn system, the ordered and disordered bcc phases occupy only a small part of the phase diagram and only limited information is available on the general scheme of the ordering transitions. However, part I of the present investigation concludes that the transition from the A2 to the D0<sub>3</sub> structure is of second order. Based on this information, the ratio of the bond exchange energies  $w_1/w_2$  can already be estimated from the work of Inden [59]. In Fig. 5b of this work (Ref. [59]), the second order A2/D0<sub>3</sub> transition is calculated in the desired region when the ratio of the bond exchange energies ( $w_1/w_2$ ) is 1. However, at lower temperatures a thin two-phase region exists between the disordered and ordered phases, A2 and D0<sub>3</sub>, respectively. At the ratio of  $w_1/w_2 = 1$  this two-phase region still extends into the stable region of the A2/D0<sub>3</sub> phases. In order to shift the two-phase region to lower temperatures, the ratio of the bond exchange energies was fixed at 0.9. Given that selection, only one ordering parameter remains to be determined. This parameter was used to fit the second order transition to the experimental data. During the final optimization, the parameters of the disordered and the ordered phase were refined simultaneously.

## 6. Results and discussion

The binary phase diagram of the Cu–Sn system calculated using the current description is shown in Fig. 2a with experimental phase diagram data from the literature superimposed in Fig. 2b. The first figure includes the calculated higher order phase transformation from the disordered A2 phase to the ordered D0<sub>3</sub> phase and the calculated metastable miscibility gap of the liquid phase as dashed lines. The calculated invariant reactions in the Cu–Sn system based on the new description are listed in Table 2, together with the experimental results reported by Saunders and Miodownik [16] and the experimental results from Part I.

The calculated phase equilibria from 0 to 30 at.% Sn are shown in Fig. 3. The dashed line indicates the calculated second order transition between the A2 and D0<sub>3</sub> phases. Verö [50] and Hamasumi [51] proposed a two-phase field between the A2 and D0<sub>3</sub> phases based on differential thermal analysis performed on alloys with between 13.8 and 15.7 at.% Sn. The observed thermal peak in this temperature range was cited as evidence for the two phase field. However, the presence of a small thermal peak can be the result of either a very narrow two phase field or a higher order phase transformation. It is interesting to note that the data points from Refs. [50,51] measured using thermal analysis are in good agreement with the high temperature XRD results detailed in Part I of this work which indicate the presence of a higher order phase transformation. Therefore, the data from Refs. [50,51] can also be interpreted in terms of a second order transformation. In part I of this work the experimental data for the A2/D0<sub>3</sub> transformation lead to a very steep transition line having even a positive curvature. However, our present ordering model can represent this transformation only with lines of negative curvature. Therefore, a close fit of the ordering data of part I is not possible. Instead, the transition line was evaluated to represent a compromise between the data of part I and the literature data [50,51].

The experimentally determined liquidus curve has a kink at approximately 1000 K, which could not be reproduced in the current optimization. It should be noted that in the work of Liu et al. [17] in which the bcc phase was experimentally investigated and the proposed A2/B2/D0<sub>3</sub> two-step higher order transformation was modeled as an A2/B2 higher order transformation, the kink in the liquidus was also not reproduced. This could be a result of the

**Table 2**

Comparison between calculated invariant phase equilibria in the Cu–Sn system with assessed results [16] and the experimental results from part I. The compositions are given in mole fraction of Sn. In this table, these phase A2 and D0<sub>3</sub> are denoted by  $\beta$  and  $\gamma$  respectively.

Equilibrium	Assessed results [16]	Experimental results, this work, part I	Calculated results, this work
Peritectic $\alpha + L \leftrightarrow \beta$	$T = 1071$ K $x_\alpha = 0.077$ $x_L = 0.155$ $x_\beta = 0.131$	$T = 1071$ K $x_\alpha = 0.077$ $x_L = 0.150$ $x_\beta = 0.126$	$T = 1071$ K $x_\alpha = 0.086$ $x_L = 0.158$ $x_\beta = 0.144$
Peritectic $\beta + L \leftrightarrow \gamma$	$T = 1028$ K $x_\beta = 0.158$ $x_L = 0.191$ $x_\gamma = 0.165$	$T = 1031$ K Degenerated, $x_\beta = x_\gamma = 0.161$ $x_L = 0.187$	$T = 1040$ K
Congruent $\gamma \leftrightarrow \varepsilon$	$T = 949$ K $x_{\varepsilon/\gamma} = 0.25$	Not investigated	$T = 945$ K $x_{\varepsilon/\gamma} = 0.25$
Metatectic $\gamma \leftrightarrow \varepsilon + L$	$T = 913$ K $x_\gamma = 0.279$ $x_\varepsilon = 0.259$ $x_L = 0.431$	$T = 922$ K $x_\gamma = 0.290$ $x_\varepsilon = 0.259$ $x_L = 0.431$	$T = 921$ K $x_\gamma = 0.276$ $x_\varepsilon = 0.250$ $x_L = 0.413$
Peritectoid $\gamma + \varepsilon \leftrightarrow \zeta$	$T = 913$ K $x_\gamma = 0.218$ $x_\varepsilon = 0.245$ $x_\zeta = 0.225$	$T = 914$ K $x_\gamma = 0.220$ $x_\varepsilon = 0.245$ $x_\zeta = 0.226$	$T = 914$ K $x_\gamma = 0.219$ $x_\varepsilon = 0.250$ $x_\zeta = 0.231$
Peritectoid $\gamma + \zeta \leftrightarrow \delta$	$T = 863$ K $x_\gamma = 0.198$ $x_\zeta = 0.209$ $x_\delta = 0.203$	$T = 876$ K $x_\gamma = 0.203$ $x_\zeta = 0.216$ $x_\delta = 0.205$	$T = 874$ K $x_\gamma = 0.200$ $x_\zeta = 0.231$ $x_\delta = 0.212$
Eutectoid $\beta \leftrightarrow \alpha + \gamma$	$T = 859$ K $x_\beta = 0.149$ $x_\alpha = 0.091$ $x_\gamma = 0.160$	$T = 839$ K Degenerated, $x_\beta = x_\gamma = 0.165$ $x_\alpha = 0.091$	$T = 892$ K
Eutectoid $\zeta \leftrightarrow \delta + \varepsilon$	$T = 855$ K $x_\zeta = 0.217$ $x_\delta = 0.208$ $x_\varepsilon = 0.245$	$T = 862$ K $x_\zeta = 0.243$ $x_\delta = 0.21$ $x_\varepsilon = 0.245$	$T = 862$ K $x_\zeta = 0.231$ $x_\delta = 0.212$ $x_\varepsilon = 0.250$
Eutectoid $\gamma \leftrightarrow \alpha + \delta$	$T = 793$ K $x_\gamma = 0.165$ $x_\alpha = 0.091$ $x_\delta = 0.204$	$T = 791$ K $x_\gamma = 0.175$ $x_\alpha = 0.091$ $x_\delta = 0.206$	$T = 791$ K $x_\gamma = 0.170$ $x_\alpha = 0.091$ $x_\delta = 0.212$
Peritectoid $\varepsilon + L \leftrightarrow \eta$	$T = 688$ K $x_\varepsilon = 0.249$ $x_L = 0.867$ $x_\eta = 0.435$	$T = 681$ K $x_\varepsilon = 0.253$ $x_L = 0.867$ $x_\eta = 0.446$	$T = 685$ K $x_\varepsilon = 0.250$ $x_L = 0.868$ $x_\eta = 0.455$
Eutectoid $\delta \leftrightarrow \alpha + \varepsilon$	$T = 623$ K $x_\delta = 0.205$ $x_\alpha = 0.062$ $x_\varepsilon = 0.245$	$T$ not measured, $x_\delta = 0.208$ $x_\alpha = 0.062$ $x_\varepsilon = 0.245$	$T = 625$ K $x_\delta = 0.212$ $x_\alpha = 0.062$ $x_\varepsilon = 0.250$
Eutectic $L \leftrightarrow \eta + (\text{Sn})$	$T = 500$ K $x_L = 0.987$ $x_\eta = 0.455$ $x_{(\text{Sn})} = 1.00$	Not investigated	$T = 498$ K $x_L = 0.979$ $x_\eta = 0.455$ $x_{(\text{Sn})} = 0.999$
Peritectoid $\varepsilon + \eta \leftrightarrow \eta'$	$T = 462$ K $x_{\eta/\eta'} = 0.455$	Not investigated	$T = 461$ K $x_\varepsilon = 0.250$ $x_\eta = 0.455$ $x_{\eta'} = 0.454$
Eutectoid $\eta \leftrightarrow \eta' + (\text{Sn})$	$T = 461$ K $x_{\eta/\eta'} = 0.455$	Not investigated	$T = 459$ K $x_\eta = 0.455$ $x_{\eta'} = 0.455$ $x_{(\text{Sn})} = 1$

limitations of the semi-empirical model used to describe the higher order phase transformation.

The calculated enthalpy of mixing of the Cu–Sn liquid alloys in comparison with literature data is shown in Fig. 4. There is generally a good agreement with the experimental data although no temperature dependence of the molar enthalpy of mixing of the liquid phase was modeled. The only work which models a temperature dependence of the molar enthalpy of mixing of the liquid phase is that of Gierlotka et al. [11]. This was based on the calorimetric measurements of Itagaki and Yazawa [29] at 1373 K and on the measurements of Lee et al. [27] at 997 K. However, in this temperature range, no temperature dependence of the mixing enthalpy was found by Flandorfer et al. [25]. The work of Flandorfer

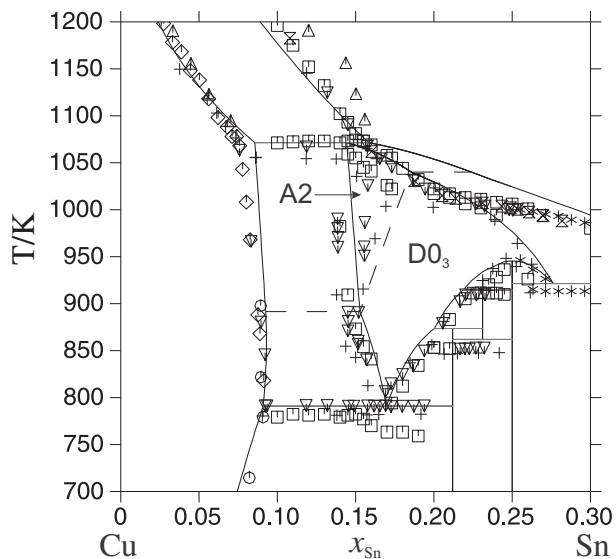


**Fig. 3.** Calculated Cu–Sn phase diagram from  $x_{\text{Sn}} = 0$  to  $x_{\text{Sn}} = 0.3$  and from 700 to 1200 K. The symbols for the experimental literature data are the same as those shown in Fig. 2b.

et al. [25], however, does indicate a temperature dependence in the range from 773 to 973 K but no obvious temperature dependence at higher temperatures. In Ref. [25], the  ${}^0W$ ,  ${}^1W$  and  ${}^2W$  parameters, where  $W = L + T \cdot \partial L / \partial T$ , were modeled as quadratic functions of temperature. These functions were shown to well reproduce the experimentally determined mixing enthalpies. To model the temperature dependence indicated in the work of Flandorfer et al. [25], each of the three  ${}^0L_{\text{Cu,Sn}}^{\text{liq}}$ ,  ${}^1L_{\text{Cu,Sn}}^{\text{liq}}$ , and  ${}^2L_{\text{Cu,Sn}}^{\text{liq}}$  binary interaction parameters for the liquid phase would need to be modeled as  $L = a + bT + cT \ln T + DT^2$ , thereby increasing the total number of variables by 6. However, even if the calorimetric data of Flandorfer [25] are taken together with the results of Kleppa at 723 K [26], there is not sufficient data to optimize these additional 6 coefficients of the liquid phase. Therefore, the experimentally observed temperature dependence of the mixing enthalpy of the liquid phase was not modeled in the present work as more experimental data is required.

The experimentally measured positive values of the enthalpy of mixing of the liquid phase for Sn rich compositions may imply the

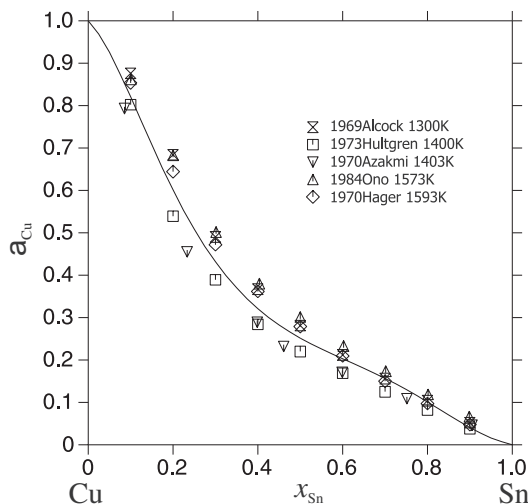


**Fig. 5.** Calculated activities of Cu in liquid Cu–Sn alloys at 1400 K in comparison with experimental data [23,32–35]. Reference state: pure liquid components.

presence of a miscibility gap in the liquid phase at lower temperatures. The calculated metastable miscibility gap in the liquid phase shown in Fig. 2a confirms this implication.

The calculated activities of Cu and Sn in the liquid phase are shown in Figs. 5 and 6, respectively, with the superimposed experimental data from the literature. Once again, a good agreement is shown between the calculations and the activity data from the experimental works.

The calculated activity of Sn in the (Cu) phase in comparison with experimental data [42–44] is shown in Fig. 7. Good agreement is shown with the experimental works of Refs. [43,44].

The enthalpies of formation of alloys in the Cu–Sn system calculated at 673 K are presented in Fig. 8 compared to the literature data. The calculated enthalpies of formation are also compared with the literature data in Table 3.

The metastable phase diagram of the bcc-based phases in the Cu-rich part of the system Cu–Sn is shown in Fig. 9. The Sn-rich part of the metastable bcc phase is dominated by a large miscibility gap with the consolute point at about 5070 K at 84 at.% Sn. The Cu-rich and Sn-rich composition sets of the A2 phase are indicated with a prime and double prime, respectively. In the

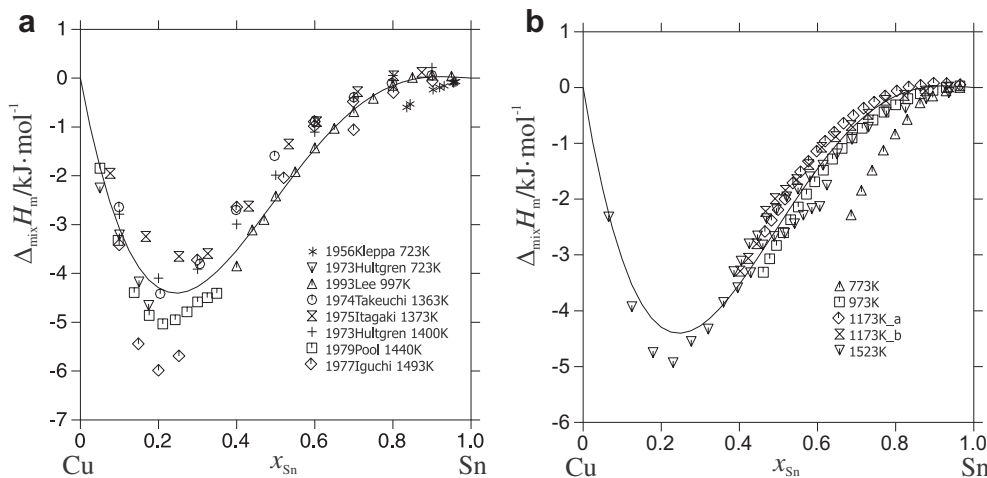


**Fig. 4.** Calculated enthalpy of mixing for the Cu–Sn liquid alloys in comparison with literature data: (a) in comparison with [23,26–31]; (b) in comparison with [25]. Reference state: pure liquid components.

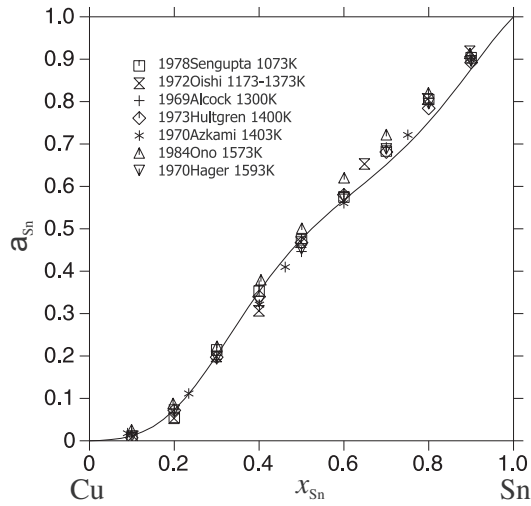


Fig. 6. Calculated activities of Sn in liquid Cu–Sn alloys at 1400 K in comparison with experimental data [23,32–37]. Reference state: pure liquid components.

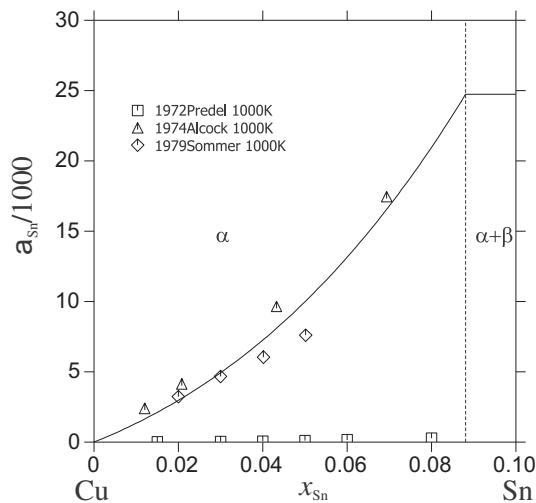


Fig. 7. Calculated activity of Sn in the (Cu) solid solution at 1000 K in comparison with literature data [42–44]. Reference state: Cu (fcc) and Sn (bct).

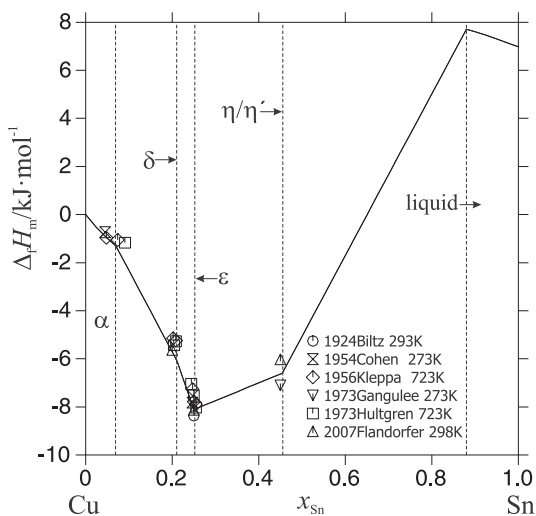


Fig. 8. Calculated enthalpies of formation of Cu–Sn alloys at 673 K in comparison with experimental data from literature [23,24,38–41]. Reference state: Cu (fcc) and Sn (bct).

Table 3

Experimentally determined enthalpies of formation and reaction of Cu–Sn binary compounds along with their corresponding values calculated using the present description. The values with \* are obtained by interpolation of the reported data. Reference state: Cu (fcc) and Sn (bct).

Phase	Symbol	Temperature/K	Values J/mol	Reference
$\delta$ (Cu <sub>41</sub> Sn <sub>11</sub> )	$\Delta_f H_m^\delta$	723	–4990*	[40]
		723	–5205*	[23]
		298	–5700	[24]
		723	–6116	This work
$\epsilon$ (Cu <sub>3</sub> Sn)	$\Delta_f H_m^\epsilon$	293	–8368	[38]
		273	–7824	[39]
		723	–7777	[40]
		723	–7531	[23]
		298	–8200	[24]
		723	–8113	This work
$\eta'$ (Cu <sub>6</sub> Sn <sub>5-L</sub> )	$\Delta_f H_m^{\eta'}$	273	–7033	[41]
		273	–7130	This work
$\eta$ (Cu <sub>6</sub> Sn <sub>5-H</sub> )	$\Delta_f H_m^\eta$	298	–6100	[24]
		298	–6600	This work
$\eta \rightarrow \eta'$	$\Delta_r H_m^{\eta \rightarrow \eta'}$	273	–265	[41]
		273	–530	This work

temperature range shown in the diagram the Sn-rich A2 phase consists almost of pure tin. In the Cu-rich part of the diagram the disordered bcc phase and its three ordered descendants, B32, D0<sub>3</sub>, and the LiMgPdSn-type phase are shown. The dashed lines between these phase regions denote second order transitions. At temperatures below 400 K in the range of 5–7 at.% Sn, a narrow two-phase region between the A2 and the D0<sub>3</sub> phase is present. However, the position of this two-phase region is very sensitive with regard to the ratio of the bond exchange energies. If  $w_1/w_2$  is slightly higher than one, the two-phase region will cross the stable A2/D0<sub>3</sub> phase region (cf. Fig. 3) but its width will be much less than 1 mol percent which is difficult to verify experimentally.

The sublattice occupations in the bcc-based structures of the metastable system at 1000 K are shown in Fig. 10. The site fractions of tin in the four sublattices, indicated by the roman numerals, are given as a function of the composition of the solid solutions in the disordered and ordered states, respectively. Within the depicted composition interval four phases with different order exist. At a transition point where a phase undergoes a second order transformation into a state of different order both states have the same Gibbs energy. In view of Equation (8) this means that the site

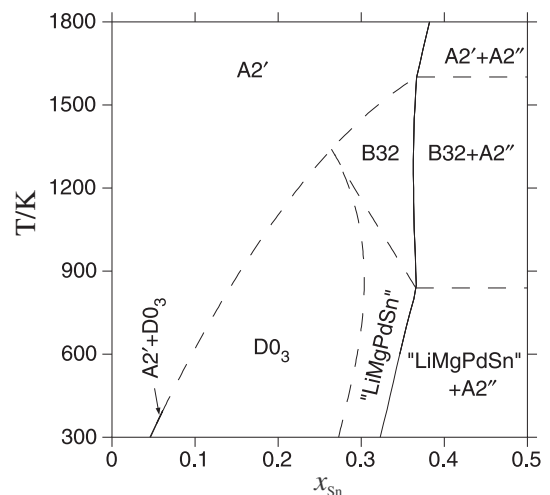


Fig. 9. Metastable phase diagram of the bcc-based phases in the Cu-rich part of the Cu–Sn system.

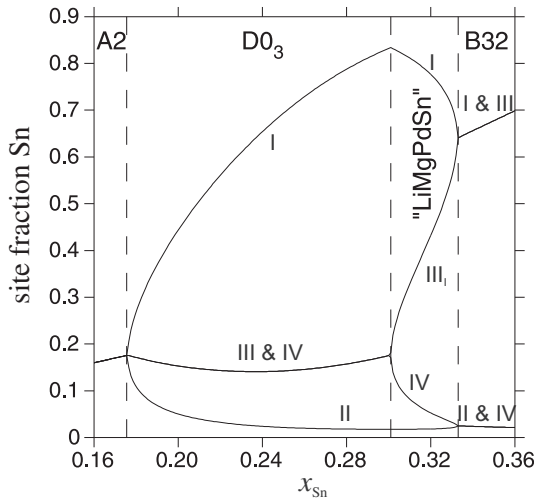


Fig. 10. Sublattice occupation in the bcc-based structures of the metastable system at 1000 K. The roman numerals denote the four sublattices.

fractions of both phases must approach the same values in the respective sublattices. Therefore, the curves for the site fractions in Fig. 10 pass through the respective branching points at the phase transitions which are indicated by dashed lines.

On this occasion it is appropriate to comment on a wrong statement given by Witusiewicz et al. [63] in their paper on phase equilibria in binary and ternary systems with chemical and magnetic ordering. Based on a few example calculations they conclude that “if the B2 structure does not form, e.g. in Fe-33.0 at.% Al, the direct transformation from A2 to D0<sub>3</sub> (L<sub>21</sub>) cannot be accomplished through smooth parabolic branching, ...”. These authors may not have been aware of the systematic study of Inden [59] who clearly pointed out that depending on the ratio of the bond exchange energies first order as well as second order transitions can be achieved between the A2 and D0<sub>3</sub> structures. Within a certain range of the bond exchange energies it is even possible that the character of this transformation changes as a function of temperature from first to second order. The order/disorder model of the present work gives an accurate example for this case. In the metastable phase diagram, Fig. 9, a second order transition between A2 and D0<sub>3</sub> is present at higher temperatures while at lower temperatures a thin two-phase field is present. Fig. 10 illustrates that in the temperature range where second order transformations are present, the site fractions change continuously at the transition points between adjacent phases.

## 7. Conclusion

A self-consistent thermodynamic description of the Cu–Sn system which models for the first time the higher order phase transformation from the disordered  $\beta$  phase with BCC structure to the ordered  $\gamma$  phase with D0<sub>3</sub> structure has been obtained. The calculated results agree well with literature information and reproduce the phase relations, thermodynamic, and thermochemical data satisfactorily.

## Acknowledgment

The authors would like to thank the German Research Foundation (DFG) Priority Program 1473 WenDeLib–Materials with New design for Improved Lithium Ion Batteries for the financial support. Special thanks are extended to Professor Hans J. Seifert, to

Dr. Andrew Watson for supplying the COST 531 Cu–Sn description with the agreement of Dr. Alan Dinsdale.

## Appendix A. Optimized thermodynamic parameters of the Cu–Sn system

**Liquid:** Model (Cu, Sn)

$${}^0G_{\text{Cu}}^{\text{liq}} - H_{\text{Cu}}^{\text{SER}} = \text{GLIQU}$$

$${}^0G_{\text{Sn}}^{\text{liq}} - H_{\text{Sn}}^{\text{SER}} = \text{GLIQSN}$$

$${}^0L_{\text{Cu,Sn}}^{\text{liq}} = -9935.17052 - 5.1572292T$$

$${}^1L_{\text{Cu,Sn}}^{\text{liq}} = -21571.2079 + 4.8428506T$$

$${}^2L_{\text{Cu,Sn}}^{\text{liq}} = -11005.7526 - 2.6059799T$$

**$\alpha$  (fcc):** Model (Cu,Sn)

$${}^0G_{\text{Cu}}^{\text{fcc}} - H_{\text{Cu}}^{\text{SER}} = \text{GHSERCU}$$

$${}^0G_{\text{Sn}}^{\text{fcc}} - H_{\text{Sn}}^{\text{SER}} = \text{GFCCSN}$$

$${}^0L_{\text{Cu,Sn}}^{\text{fcc}} = -10000 + 0.2T$$

$${}^0L_{\text{Cu,Sn}}^{\text{fcc}} = -18500 + 6.8T$$

**$\beta$  (BCC-A2):** Model (Cu,Sn)

$${}^0G_{\text{Cu}}^{\text{bcc-A2}} - H_{\text{Cu}}^{\text{SER}} = \text{GBCCCU}$$

$${}^0G_{\text{Sn}}^{\text{bcc-A2}} - H_{\text{Sn}}^{\text{SER}} = \text{GBCCSN}$$

$${}^0L_{\text{Cu,Sn}}^{\text{bcc-A2}} = 5224$$

$${}^1L_{\text{Cu,Sn}}^{\text{bcc-A2}} = -95350 + 9.28T$$

$${}^2L_{\text{Cu,Sn}}^{\text{bcc-A2}} = 29870$$

**$\gamma$  (BCC-4SL):** Model (Cu,Sn)<sub>0.25</sub>; (Cu,Sn)<sub>0.25</sub>; (Cu,Sn)<sub>0.25</sub>; (Cu,Sn)<sub>0.25</sub>

Note that this phase has a contribution from the disordered part BCC-A2. Parameters that are identical for symmetry reason are listed only once.

$${}^0G_{\text{Cu:Cu:Cu:Cu}}^{\text{4SL}} = 0$$

$${}^0G_{\text{Cu:Cu:Sn:Sn}}^{\text{4SL}} = -4W1$$

$${}^0G_{\text{Cu:Sn:Cu:Sn}}^{\text{4SL}} = -2W1 - 3W2$$

$${}^0G_{\text{Cu:Cu:Cu:Sn}}^{\text{4SL}} = -2W1 - 1.5W2$$

$${}^0G_{\text{Sn:Sn:Sn:Cu}}^{\text{4SL}} = -2W1 - 1.5W2$$

$${}^0G_{\text{Sn:Sn:Sn:Sn}}^{\text{4SL}} = 0$$

**Sn (BCT):** Model (Sn)

$${}^0G_{\text{Sn}}^{\text{bct}} - H_{\text{Sn}}^{\text{SER}} = \text{GHSERSN}$$

**$\delta$  (Cu<sub>41</sub>Sn<sub>11</sub>):** Model (Cu)<sub>0.788</sub>(Sn)<sub>0.212</sub>

$${}^0G_{\text{Cu}_41\text{Sn}_{11}}^{\text{Cu}} - 0.788{}^0G_{\text{Cu}}^{\text{fcc}} - 0.212{}^0G_{\text{Sn}}^{\text{bct}} = -6116 - 1.83T$$

**$\zeta$  (Cu<sub>10</sub>Sn<sub>3</sub>):** Model (Cu)<sub>0.769</sub>(Sn)<sub>0.231</sub>

$${}^0G_{\text{Cu}_{10}\text{Sn}_3}^{\text{Cu}} - 0.769{}^0G_{\text{Cu}}^{\text{fcc}} - 0.231{}^0G_{\text{Sn}}^{\text{bct}} = -6382 - 2.048T$$

**$\epsilon$  (Cu<sub>3</sub>Sn):** Model (Cu)<sub>0.75</sub>(Sn)<sub>0.25</sub>

$${}^0G_{\text{Cu}_3\text{Sn}}^{\text{Cu}} - 0.75{}^0G_{\text{Cu}}^{\text{fcc}} - 0.25{}^0G_{\text{Sn}}^{\text{bct}} = -8113 - 0.566T$$

**$\eta$  (Cu<sub>6</sub>Sn<sub>5</sub>-H):** Model (Cu)<sub>0.545</sub>(Cu,Sn)<sub>0.122</sub>(Sn)<sub>0.333</sub>

For this phase, only the  ${}^0G_{\text{Cu:Sn:Sn}}^{\text{Cu}_6\text{Sn}_5\text{-H}}$  parameter was modified from the COST 531 [19] database, the rest two parameters are kept not changed.

$${}^0G_{\text{Cu:Cu:Sn}}^{\text{Cu}_6\text{Sn}_5\text{-H}} - 0.667{}^0G_{\text{Cu}}^{\text{fcc}} - 0.333{}^0G_{\text{Sn}}^{\text{bct}} = 3200 + 2T$$

$${}^0G_{\text{Cu:Sn:Sn}}^{\text{Cu}_6\text{Sn}_5\text{-H}} - 0.545{}^0G_{\text{Cu}}^{\text{fcc}} - 0.455{}^0G_{\text{Sn}}^{\text{bct}} = -6600.0586 - 0.74899T$$

$${}^0G_{\text{Cu:Cu:Sn:Sn}}^{\text{Cu}_6\text{Sn}_5\text{-H}} = -8300$$

$\eta'$  (**Cu<sub>6</sub>Sn<sub>5</sub>-L**): Model (Cu)<sub>0.545</sub>(Cu,Sn)<sub>0.455</sub>

$${}^0G_{\text{Cu:Cu}}^{\text{Cu}_6\text{Sn}_5\text{-L}} - H_{\text{Cu}}^{\text{SER}} = \text{GHSERCU} + 1000$$

$${}^0G_{\text{Cu:Sn}}^{\text{Cu}_6\text{Sn}_5\text{-L}} - 0.545{}^0G_{\text{Cu}}^{\text{fcc}} - 0.455{}^0G_{\text{Sn}}^{\text{bct}} = -7129.7 + 0.4059T$$

[19]

Symbols

$$298.14 \text{ K} \leq T < 1357.77 \text{ K}$$

$$\begin{aligned} \text{GHSERCU} = & -7770.458 + 130.485235T - 24.112392T \ln T \\ & - 2.65684 \times 10^{-3}T^2 + 1.29223 \times 10^{-7}T^3 \\ & + 52478T^{-1} \end{aligned}$$

$$1357.77 \text{ K} \leq T < 3200 \text{ K}$$

$$\begin{aligned} \text{GHSERCU} = & -13542.026 + 183.803828T - 31.38T \ln T \\ & + 3.64167 \times 10^{29}T^{-9} \end{aligned}$$

$$100 \text{ K} \leq T < 250 \text{ K}$$

$$\begin{aligned} \text{GHSERSN} = & -7958.517 + 122.765451T - 25.858T \ln T \\ & + 5.1185 \times 10^{-4}T^2 - 3.192767 \times 10^{-6}T^3 \end{aligned}$$

$$250 \text{ K} \leq T < 505.08 \text{ K}$$

$$\begin{aligned} \text{GHSERSN} = & -5855.135 + 65.443315T - 15.961T \ln T \\ & - 1.88702 \times 10^{-2}T^2 + 3.121167 \times 10^{-6}T^3 \\ & - 61960T^{-1} \end{aligned}$$

$$505.08 \text{ K} \leq T < 800 \text{ K}$$

$$\begin{aligned} \text{GHSERSN} = & 2524.724 + 4.005269T - 8.2590486T \ln T \\ & - 1.6814429 \times 10^{-2}T^2 + 2.623131 \times 10^{-6}T^3 \\ & - 1081244T^{-1} - 1.2307 \times 10^{25}T^{-9} \end{aligned}$$

$$800 \text{ K} \leq T < 3000 \text{ K}$$

$$\begin{aligned} \text{GHSERSN} = & -8256.959 + 138.99688T - 28.4512T \ln T \\ & - 1.2307 \times 10^{25}T^{-9} \end{aligned}$$

$$298.15 \text{ K} \leq T < 1357.77 \text{ K}$$

$$\begin{aligned} \text{GLIQU} = & \text{GHSERCU} + 12964.735 - 9.511904T - 5.849 \\ & \times 10^{-21}T^7 \end{aligned}$$

$$1357.77 \text{ K} \leq T < 3200.00 \text{ K}$$

$$\text{GLIQU} = -46.545 + 173.881484 \times T - 31.38T \ln T$$

$$100 \text{ K} \leq T < 505.08 \text{ K}$$

$$\begin{aligned} \text{GLIQSN} = & \text{GHSERSN} + 7103.092 - 14.087767T + 1.47031 \\ & \times 10^{-18}T^7 \end{aligned}$$

$$505.08 \text{ K} \leq T < 800 \text{ K}$$

$$\begin{aligned} \text{GLIQSN} = & 9496.31 - 9.809114T - 8.2590486T \ln T \\ & - 1.6814429 \times 10^{-2}T^2 + 2.623131 \times 10^{-6}T^3 \\ & - 1081244T^{-1} \end{aligned}$$

$$800 \text{ K} \leq T < 3000 \text{ K}$$

$$\begin{aligned} \text{GLIQSN} = & -1285.372 + 125.182498T - 28.4512T \ln T \\ & 298.15 \text{ K} \leq T < 1357.77 \text{ K} \end{aligned}$$

$$\text{GBCCCU} = \text{GHSERCU} + 4017 - 1.255T$$

$$100 \text{ K} \leq T < 3000 \text{ K:}$$

$$\text{GBCCSN} = \text{GHSERSN} + 4400 - 6T$$

$$100 \text{ K} \leq T < 3000 \text{ K:}$$

$$\text{GFCCSN} = \text{GHSERSN} + 5510 - 8.46T$$

$$W1 = 4297.5$$

$$W2 = 4775$$

## References

- [1] Yang W, Messler R, Felton L. *J Electron Mater* 1994;23(8):765–72.
- [2] Lee C-B, Jung S-B, Shin Y-E, Shur C-C. *Mater Trans JIM* 2001;42(5):751–5.
- [3] Takemoto T, Matsunawa A, Takahashi M. *J Mater Sci* 1997;32(15):4077–84.
- [4] Kim MG, Sim S, Cho J. *Adv Mater* 2010;22(45):5154–8.
- [5] Kepler KD, Vaughney JT, Thackeray MM. *J Power Sources* 1999;81:383–7.
- [6] Tamura N, Ohshita R, Fujimoto M, Fujitani S, Kamino M, Yonezu I. *J Power Sources* 2002;107(1):48–55.
- [7] Xue LG, Fu ZH, Yao Y, Huang T, Yu AS. *Electrochim Acta* 2010;55(24):7310–4.
- [8] Kamali AR, Fray DJ. *Rev Adv Mater Sci* 2011;27(1):14–24.
- [9] Shim JH, Oh CS, Lee BJ, Lee DNZ. *Metallkd* 1996;87(3):205–12.
- [10] Miettinen J. *Metall Mater Trans A* 2002;33(6):1639–48.
- [11] Gierlotka W, Chen SW, Lin SK. *J Mater Res* 2007;22(11):3158–65.
- [12] Raynor GV. The Cu-Sn phase diagram. In: Annotated equilibrium diagram series, vol. 2. London: The Institute of Metals; 1944.
- [13] Hansen M. *Der Aufbau der Zweistofflegierungen*. Berlin: Springer-Verlag OHG; 1936. p. 634–47.
- [14] Hansen M, Andrerkko K. *Constitution of binary alloys*. 2nd ed. New York: McGraw-Hill; 1958. p. 633–8.
- [15] Saunders N, Miodownik AP. Cu-Sn (copper-tin). In: Massalski TB, editor. *Binary alloy phase diagrams*, vol. 2. Materials Park, OH: ASM International; 1990. p. 1481–3.
- [16] Saunders N, Miodownik AP. Cu-Sn (copper-tin). In: Subramanian PR, Chakrabarti DJ, Laughlin DE, editors. *Phase diagrams of binary copper alloys*. Materials Park, OH: ASM International; 1994. p. 412–8.
- [17] Liu XJ, Wang CP, Ohnuma I, Kainuma R, Ishida K. *Metall Mater Trans A* 2004;35A(6):1641–54.
- [18] Li M, Du ZM, Guo CP, Li CR. *J Alloys Compd* 2009;477(1–2):104–17.
- [19] Lee BJ, Cu-Sn. In: Dinsdale AT, Watson A, Kroupa A, Vrestal J, Zemanova A, Vizdal J, editors. *COST action 531-atlas of phase diagrams for lead-free soldering*, vol. 1. Czech Republic: COST Office; 2008. p. 91–3.
- [20] Wang JA, Liu CL, Leinenbach C, Klotz UE, Uggowitzer PJ, Löffler JF. *Calphad* 2011;35(1):82–94.
- [21] Moon K, Boettinger W, Kattner U, Biancanello F, Handwerker C. *J Electron Mater* 2000;29(10):1122–36.
- [22] Hultgren RR, Desai PD. *Selected thermodynamic values and phase diagrams for copper and some of its binary alloys*. New York: International Copper Research Association; 1971.
- [23] Hultgren R, Desai PD, Hawkins DT, Gleiser M, Kelley KK. *Selected values of the thermodynamic properties of binary alloys*. Metals Park, OH: American Society for Metals; 1973.
- [24] Flandorfer H, Saeed U, Luef C, Sabbar A, Ipser H. *Thermochim Acta* 2007;459(1–2):34–9.
- [25] Flandorfer H, Luef C, Saeed U. *J Non-Cryst Solids* 2008;354(26):2953–72.
- [26] Kleppa OJ. *J Phys Chem* 1956;60(7):842–6.
- [27] Lee JJ, Kim BJ, Min WS. *J Alloys Compd* 1993;202:237–42.
- [28] Takeuchi S, Uemura O, Ikeda S. *Sci Rep Tohoku Imp Univ* 1974;25A:41–55.
- [29] Itagaki K, Yazawa A. *Trans Jpn Inst Met* 1975;16(11):679–86.
- [30] Pool MJ, Predel B, Schultheiss E. *Thermochim Acta* 1979;28(2):349–58.
- [31] Iguchi Y, Shimoji H, Ban-Ya S, Fuwa T. *Tetsu-to-Hagane* 1977;63:275–84.
- [32] Alcock CB, Sridhar R, Svedberg RC. *Acta Mater* 1969;17(7):839–44.
- [33] Ono K, Nishi S, Oishi T. *Trans Jpn Inst Met* 1984;25(11):810–4.
- [34] Azakami T, Yazawa A. *J Min Met Inst Jpn* 1970;86:377–82.
- [35] Hager J, Howard S, Jones J. *Metall Mater Trans* 1970;1(2):415–22.
- [36] Sengupta A, Jag Annathan K, Ghosh A. *Metall Mater Trans B* 1978;9(2):141–3.
- [37] Oishi T, Moriyama J. *J Jpn Inst Met* 1972;36:481–845.

- [38] Biltz W. *Z Anorg Allg Chem* 1924;134(1):25–36.
- [39] Cohen JB, Leach JSL, Bever MBJ. *Metals* 1954;6:1257–8.
- [40] Kleppa OJ. *J Phys Chem* 1956;60(7):858–63.
- [41] Gangulee A, Das G, Bever M. *Metall Mater Trans* 1973;4(9):2063–6.
- [42] Predel B, Schallner U. *Mater Sci Eng* 1972;10(0):249–58.
- [43] Sommer F, Balbach W, Predel B. *Thermochim Acta* 1979;33(0):119–26.
- [44] Alcock CB, Jacob KT. *Acta Mater* 1974;22(5):539–44.
- [45] Yassin A, Castanet R. *J Alloys Compd* 2000;307:191–8.
- [46] Bastow BD, Kirkwood DH. *J Inst Met* 1971;99:277–83.
- [47] Raper AR. *J Inst Met* 1927;38:217–40.
- [48] Stockdale DJ. *Inst Met* 1925;34:111–24.
- [49] Heycock CT, Neville FH. *Philos Trans R Soc London Ser A* 1897;A189:47–51. 62–66.
- [50] Verö J. *Z Anorg Allg Chem* 1934;218(4):402–24.
- [51] Hamasumi M. *Nippon Kinzoku Gakkaishi* 1938;2(4):147–61.
- [52] Bauer OZ. *Allg Mikrobiol* 1923;15:119–25. 191–195.
- [53] Hasse C, Pawlek F. *Z Allg Mikrobiol* 1936;28:73–80.
- [54] Redlich O, Kister AT. *Ind Eng Chem* 1948;40(2):345–8.
- [55] Liu XJ, Liu HS, Ohnuma I, Kainuma R, Ishida K, Itabashi S, et al. *J Electron Mater* 2001;30(9):1093–103.
- [56] Eberz U, Seelentag W, Schuster HU. *Z Naturforsch B* 1980;35(11):1341–3.
- [57] Ansara I, Dupin N, Sundman B. *Calphad* 1997;21(4):535–42.
- [58] Richards MJ, Cahn JW. *Acta Metall* 1971;19(11):1263.
- [59] Inden G. *Acta Metall* 1974;22(8):945–51.
- [60] Hallstedt B, Kim O. *Int J Mater Res* 2007;98(10):961–9.
- [61] Hallstedt B, Dupin N, Hillert M, Höglund L, Lukas HL, Schuster JC, et al. *Calphad* 2007;31(1):28–37.
- [62] Sundman B, Jansson B, Andersson JO. *Calphad* 1985;9(2):153–90.
- [63] Witusiewicz VT, Bondar AA, Hecht U, Velikanova TY. *J Phase Equilib Diff* 2011; 32(4):329–49.